Hyperfine interactions in a gadolinium-based MRI contrast agent: High-frequency modulations from ab initio simulations

Aurélie Lasoroski, Rodolphe Vuilleumier, and Rodolphe Pollet

Citation: J. Chem. Phys. **139**, 104115 (2013); doi: 10.1063/1.4820791
View online: http://dx.doi.org/10.1063/1.4820791
View Table of Contents: http://jcp.aip.org/resource/1/JCPSA6/v139/i10
Published by the AIP Publishing LLC.

Hyperfine interactions in a gadolinium-based MRI contrast agent: High-frequency modulations from *ab initio* simulations

Aurélie Lasoroski,[1,2] Rodolphe Vuilleumier,[2,3] and Rodolphe Pollet[1,a)]
[1]*DSM/IRAMIS/SIS2M (CEA-CNRS UMR3299), Commissariat à l'Énergie Atomique, 91191 Gif-sur-Yvette, France*
[2]*École Normale Supérieure, Département de Chimie, ENS-CNRS-UPMC UMR8640, 75005 Paris, France*
[3]*UPMC Univ Paris 06, 4, Place Jussieu, 75005 Paris, France*

(Received 14 June 2013; accepted 16 August 2013; published online 13 September 2013)

Hyperfine coupling tensors of the water molecule coordinated to the Prohance contrast agent in liquid water were calculated within and beyond the point dipole approximation along an *ab initio* molecular dynamics trajectory. We observe the non-equivalence at short time scales on structural as well as magnetodynamical properties of inner sphere water protons due to hydrogen bonds formation with the solvent. In addition, the influence of ultrafast internal motions on the anisotropic, dipolar, contribution to hyperfine couplings was probed thanks to a decomposition of its fluctuations in terms of a small set of meaningful collective variables. © *2013 AIP Publishing LLC*. [http://dx.doi.org/10.1063/1.4820791]

INTRODUCTION

In more than one third of clinical applications of magnetic resonance imaging (MRI) around the world, images of examined tissues are enhanced by the injection of so-called T_1 paramagnetic contrast agents (CA) which are mostly gadolinium(III) complexes. Their diffusion in the human body indeed causes a local shortening of the spin-lattice relaxation time T_1 of the protons of water molecules, especially for those belonging to the inner sphere (IS) of the CA due to their close proximity to the unpaired electrons of the paramagnetic center. The hyperfine interaction between nuclear and electron spins is then particularly strong. Its modulations, through molecular random motions, can increase the probability of NMR transitions and, on the macroscopic scale, the recovery of the longitudinal component of the bulk magnetization vector at equilibrium.[1]

In small Gd(III) chelates, molecular tumbling and IS water exchange have been identified as the molecular motions that contribute the most to the spectral density function of the electron magnetic field at relevant combinations of the nuclear Larmor frequencies, providing efficient IS relaxation pathways. In order to find compounds surpassing these clinically approved CAs, the rotational correlation time has been further optimized by anchoring small Gd(III) complexes to macromolecules including polymers, dendrimers, or proteins.[2] However, not only is the influence of the water exchange rate more important than for monomeric Gd(III) complexes, but also the internal flexibility of the macromolecular chelates (e.g., of the polymer chain or the linker group to the dendrimer) becomes more limitative with respect to the proton relaxation process. In order to model these internal motions, Lipari and Szabo[3,4] have expressed the spectral density function in terms of two correlation times corresponding to both slow global (i.e., macromolecular) and fast local (i.e., Gd monomeric) motions. The more subtle effects of vibrations, which are even faster motions, are better incorporated in a vibrationally averaged hyperfine coupling tensor if the latter remains axially symmetric (i.e., contains two degenerate eigenvalues).[5–7]

These ultrafast vibrational motions occur in the extreme narrowing regime where correlation times are very short. This regime is not seen in NMR experiments but perfectly suits the simulation lengths that can be typically reached with *ab initio* molecular dynamics (AIMD) simulations, which then allow to study these motions in details. The length of these simulations indeed rarely exceeds a hundred picoseconds because of the high computational cost resulting from the simultaneous propagation of nuclear and electronic degrees of freedom.[8] In the Car-Parrinello (CP) method, electronic forces are calculated within density functional theory (DFT) and an extended lagrangian is used. When Kohn-Sham orbitals are expanded in terms of plane waves, such as in the CPMD code,[9] AIMD simulations of realistic systems in solutions can be efficiently performed on parallel computer architectures.[10]

Unfortunately, on-the-fly calculations of hyperfine tensors along the AIMD trajectories would suffer from errors due to semi-local approximations of the exchange-correlation density functional and to the pseudopotential approximation, often required for such demanding simulations. Instead, one could compute hyperfine tensors at a higher level of theory for a selection of configurations extracted from the CP trajectory. This strategy has been used by Yazyev *et al.* in the case of the aquo gadolinium ion.[11] For the $[Gd(DOTA)(H_2O)]^-$ complex, they alternatively used a classical molecular dynamics trajectory based on a non-polarizable force field.[12]

In this work, we report the results of a mixed quantum-chemistry/AIMD approach applied to the [Gd(HPDO3A)(H_2O)] complex (i.e., Prohance MRI contrast agent) in liquid water. This study of the relaxation properties

a)Electronic mail: rodolphe.pollet@cea.fr

of this CA follows the previous investigation by one of us and coworkers of the water exchange mechanism of two of its isomers using *ab initio* metadynamics simulations.[13] Based on a CP trajectory previously performed for the most stable, capped square antiprism (CSA), isomer at free-energy equilibrium, time-dependent hyperfine tensors have been accurately calculated and their fast dynamics has been decomposed in terms of a selection of relevant vibrational motions. In addition, we will briefly discuss the validity of the point dipole approximation to the hyperfine interaction as well as its effect on outer sphere (OS) water molecules.

THEORY

Along AIMD trajectories, the time fluctuations of the hyperfine interaction can be monitored by following the (time dependent) spin hamiltonian[14]

$$H^{hyp} = H^{cont} + H^{dip} \tag{1}$$

$$= \sum_n a_n^{cont} \mathbf{S}\cdot\mathbf{I}(n) + \sum_n \sum_{\lambda,\mu} a_{n,\lambda\mu}^{dip} \mathbf{S}_\lambda \mathbf{I}_\mu(n), \quad (\lambda,\mu = x,y,z), \tag{2}$$

which couples electron (**S**) and nuclear (**I**) spin operators through contact and dipolar contributions. From the Breit-Pauli hamiltonian, it can be shown that the coupling constant a_n^{cont} and, e.g., the coupling tensors $a_{n,xx}^{dip}$ and $a_{n,xy}^{dip}$ actually depend on the electron normalized spin density distribution $D_S(r)$, namely,

$$a_n^{cont} = \frac{8\pi}{3} g\beta g_n \beta_p D_S(\mathbf{R}_n), \tag{3}$$

$$a_{n,xx}^{dip} = 3g\beta g_n \beta_p \int \left(\frac{x_n^2 - \frac{1}{3}r_n^2}{r_n^5}\right) D_S(\mathbf{r})\mathrm{d}\mathbf{r}, \tag{4}$$

$$a_{n,xy}^{dip} = 3g\beta g_n \beta_p \int \left(\frac{x_n y_n}{r_n^5}\right) D_S(\mathbf{r})\mathrm{d}\mathbf{r}, \tag{5}$$

where g and g_n are the electron and nuclear g-factors, and β and β_p are the Bohr and nuclear magnetons. While the calculation of the contact contribution only requires the value of the electron spin density at the position of the nucleus $\mathbf{R}_n$, the electron spin delocalization throughout space is taken into account in the dipolar contribution. This differs from a purely classical model where the interaction between electron and nuclear magnetic dipoles is described by a point dipole (PD) approximation, the electron dipole being strictly localized on the metal ion.

Due to solvent and temperature effects, the fluctuations of the spin hamiltonian of Eq. (1) are induced by molecular tumbling and internal vibrations. If one assumes that both motions are decoupled, the influence of molecular vibrations can be extracted by studying the hamiltonian H^{hyp} in a fixed framework with respect to the molecule. In order to elucidate the molecular motions that induce the fluctuations of the hyperfine hamiltonian and give rise to its density of state, we decompose the fluctuations of H^{hyp} in terms of a selection of a few relevant vibrational motions. Such analysis has been, for example, performed for another magnetic property, namely, the exchange coupling constant J.[15] In the present work, effective normal modes have been extracted from the AIMD trajectory according to a method similar to the one developed by one of us and coworkers for decomposing vibrational spectra.[16] The method consists in choosing a set of internal coordinates, $\theta_i (i = 1\ldots k)$ and expressing the deviation $\delta a_n^{cont,dip}(t) = a_n^{cont,dip}(t) - \langle a_n^{cont,dip}\rangle_{vib}$ of $a_n^{cont,dip}$ around its average value as a linear combination of the internal coordinates. More particularly, we focus on the zz component of the dipolar part of the hyperfine hamiltonian, with the axis z aligned with the eigenvector corresponding to the largest eigenvalue of the tensor (which is found to be very close to the Gd-O_w direction, from Gd^{3+} to the oxygen of the water molecule),

$$\delta a_{n,zz}^{dip}(t) \approx c_{n,1}\delta\theta_1(t) + \cdots + c_{n,k}\delta\theta_k(t), \tag{6}$$

where $\delta\theta_i(t) = \theta_i(t) - \langle\theta_i\rangle_{vib}$ is also the deviation of the internal coordinate i around its average value. The coefficients $c_{n,i}$, $i = 1\ldots k$ are determined by a least squares fit, minimizing

$$\chi^2 = \frac{1}{N_t}\sum_t \left\{\delta a_{n,zz}^{dip}(t) - [c_{n,1}\delta\theta_1(t) + \cdots + c_{n,k}\delta\theta_k(t)]\right\}^2, \tag{7}$$

where t indicates the time frame in the simulation and N_t the total number of time frames.

Our spectral decomposition has been achieved by choosing a basis including the out-of-plane motion (θ_1), the Gd–O_w distance (θ_2), the difference between the (GdO_wH_1) and (GdO_wH_2) angles (θ_3), the ($H_1O_wH_2$) angle (θ_4), and the O_w–H_i distances (θ_5, θ_6). Thus θ_1, θ_2, and θ_3 describe the position and orientation of the water molecule with respect to Gd, while θ_4, θ_5, and θ_6 describe the internal motion of the water molecule. Such collective variables (CVs) have been selected for their ability to describe the main internal motions, and because they show only weak coupling as checked from the small overlap between their respective density of states.

The algebraic weight, denoted here $w_{n,i}$, of each collective variable i is written as

$$w_{n,i} = \frac{c_{n,i} \times \sqrt{\langle\delta\theta_i^2\rangle_{vib}}}{\sqrt{\sum_j c_{n,j}^2 \times \langle\delta\theta_j^2\rangle_{vib}}} \tag{8}$$

in such a way that $\sum_i w_{n,i}^2 = 1$ and that the weights are independent of the choice of units for the collective variables. With this decomposition of the fluctuations of $a_{n,zz}^{dip}$ it is possible to approximate the density of states of $a_{n,zz}^{dip}$,

$$I(\omega) = \int dt \left\langle \dot{a}_{n,zz}^{dip}\dot{a}_{n,zz}^{dip}(t)\right\rangle_{vib} e^{-i\omega t} \tag{9}$$

as

$$I_{rec}(\omega) = \sum_{i=1}^{k} c_{n,i}^2 I_i(\omega), \tag{10}$$

with

$$I_i(\omega) = \int dt\ \langle \dot{\theta}_i \dot{\theta}_i(t) \rangle_{vib}\, e^{-i\omega t}, \tag{11}$$

where we assume that the collective variables are decoupled. While it is possible to transform the internal coordinates in order to find the best set of linear combinations that ensure decoupling,[16] we preferred to keep the original internal coordinates to facilitate the interpretation of the results in terms of molecular motions.

COMPUTATIONAL DETAILS

Ab initio molecular dynamics trajectories

Car-Parrinello simulations often suffer from either too short trajectory lengths (i.e., about 10 ps), too small system sizes (e.g., too few solvation shells), or a conjunction of these two limitations. In our efforts to perform a realistic simulation of the major isomer of [Gd(HPDO3A)(H_2O)] in aqueous solution, a 15.4 Å cubic box including in addition 98 water molecules has been used, which corresponds to more than two hydration shells beyond the inner sphere of the complex. Its Kohn-Sham energy has been calculated using the PBE functional[17] and expanding orbitals in a plane wave basis set defined by a cutoff energy of 30 Ry. Core electrons have been represented by ultrasoft pseudopotentials[18] including scalar relativistic effects, with a nonlinear core correction[8] in the case of the Gd 4*f*-in-core pseudopotential. The Car-Parrinello simulation has been performed with a fictitious electron mass of 700 a.u., a time step of 6 a.u. (i.e., 0.15 fs), and Nosé–Hoover chain thermostats (with a chain length of three) both for ions (with the target temperature set to 300 K) and electrons (with the target fictitious kinetic energy set to 0.03255 a.u.) to prevent heat transfer between both subsystems. To this aim, hydrogen atoms have also been replaced by deuterium atoms. In comparison with the previous work of one of us and coworkers in these exact same conditions,[13] the simulation length has been further increased from 43 to 86 ps. Only the last 23 ps have been retained for the computation of structural and magnetic properties in the present work.

Quantum chemical calculations

Static quantum chemical calculations have been performed with the ADF software,[19–21] using Slater-type basis functions. While the large atomic number of the gadolinium ion requires a relativistic treatment, its spherical electronic configuration ($4f^7$) combined with a wide HOMO-LUMO gap does not require a spin-orbit (SO) correction even when encapsulated within a macrocyclic ligand such as HPDO3A. This is clearly demonstrated in our benchmarks performed for the calculation of hyperfine tensors (see the supplementary material[22]) and has been previously reported as small for other systems of interest.[23] Therefore, only scalar relativistic effects have been included within the Zeroth Order Regular Approximation (ZORA) to the Dirac equation. The associated all-electron TZP (for Gd) and TZ2P valence triple zeta basis sets have been chosen. Benchmark calculations for Prohance and Gd(III) aquo ion (see the supplementary material[22]) comparing spin-unrestricted DFT calculations using different exchange-correlation functionals and MP2 calculations (using ORCA package[24]) have also shown that the PBE0 approximation provided the most accurate and stable hyperfine tensors. In addition, tests have been performed to study the influence of the number of water molecules extracted from the AIMD simulation box (see the supplementary material[22]). Eventually only the molecules hydrogen-bonded to the IS water molecule can be retained to provide an accurate calculation of the hyperfine constants.

RESULTS AND DISCUSSION

Influence of hydrogen bonds

Since our analysis will mainly concern the magnetic properties of the IS water molecule, we start with a brief comparison between its MD averaged geometry and experimental data. A typical configuration of the Gd complex and the IS water molecule is shown in Fig. 1. The IS oxygen atom is found at 2.54 Å from Gd, which can be compared with the X-ray value of 2.51 Å.[25] Both hydrogens are not equivalent within the time scale of our AIMD simulation. This short-time feature has rarely been observed or discussed though we will show that it can reveal how significantly averaged and dynamical properties of hyperfine tensors are both influenced by the presence of a polar solvent. We emphasize here that taking into account entropic effects and using an explicit solvation model by performing an MD simulation seems to influence the hydrogen bonds network in comparison with geometry optimizations with a mixed cluster/continuum model. Indeed, a recent theoretical study,[26] using only two explicit OS water molecules, has reported optimized geometries with almost equivalent hydrogens atoms (i.e., distances to Gd differ by less than 0.083 Å). In our work the non-equivalence

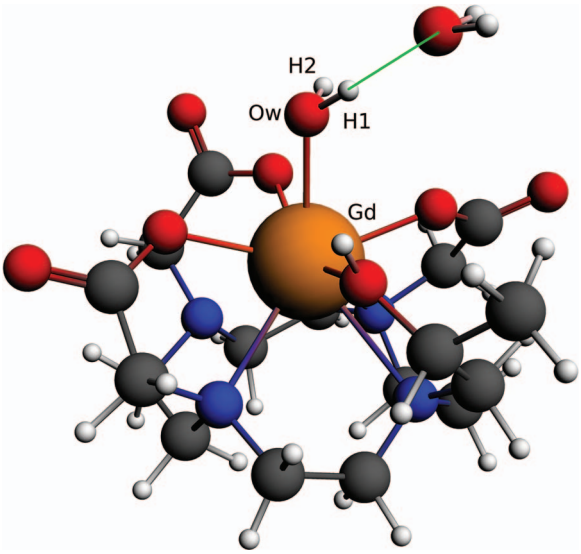

FIG. 1. [Gd(HPDO3A)(H_2O)] complex together with one hydrogen-bonded solvent molecule. The configuration has been extracted from the AIMD trajectory and is representative of the average dipole orientation (i.e., angle of 128° with respect to Gd-O_w vector).

TABLE I. Isotropic and longitudinal components of the hyperfine tensor (on the instantaneous principal axes) of the IS water molecule averaged on the 23 ps part of the Car-Parrinello trajectory with a 58 fs time interval between each configurations; fluctuations are given in parentheses.

Site	a^{cont} (MHz)	a_{zz} (MHz)
H1	0.05 (0.05)	4.98 (0.68)
H2	0.10 (0.05)	6.80 (1.13)
O_w	0.45 (0.22)	−0.65 (0.09)

of both protons stems from the orientation of the dipole moment of the IS water, which forces H1 (see Fig. 1 for the atom labelling) to be farther from the gadolinium atom (3.19 Å) and to be exposed to the solvent while H2 is closer to Gd (2.89 Å) and protected from the solvent. The best experimental value, obtained by ENDOR spectroscopy in a glassy water/methanol solution,[27] provides an intermediate distance of 3.1 ± 0.1 Å, in excellent agreement with our theoretical values. As a consequence of this proton asymmetry, much more frequent hydrogen bonds are formed between surrounding water molecules and H1 (for 91% of the 23 ps duration versus 5% for H2), as pictured in Fig. 1. This results in a slightly longer average distance to the oxygen atom, namely, 1.01 Å, versus 0.98 Å for H2.

These structural differences directly transcribe into distinct magnetic properties (see Table I). The average isotropic constant, a^{cont}, for H1 is indeed much weaker than for H2 because its larger distance from Gd implies a weaker spin polarization. The former is close to the experimental value of 0.04 MHz reported by Astashkin *et al.*[27] We note that geometry optimizations with "constrained" equivalent water protons (see above)[26] result in slightly larger values (i.e., between 0.07 and 0.11 MHz). As for the oxygen atom, the agreement with experimental data (0.46 MHz[28]) is also very good. While the contribution is larger than for hydrogen atoms, it remains rather low because its position nearly corresponds to a node of the electron spin density distribution (see Figs. 2 and 3(a)). In fact, locally, the shape of the latter almost identifies to the lone pair of the water molecule, with spins antiparallel to those of the occupied $4f_\alpha$ spinorbitals. This results from the preferential transfer of α spin electrons from the lone pair to the $5d$ spinorbitals of Gd. Actually, the same mechanism occurs for the carboxylate and amino groups of the chelate (see Figs. 2, 3(a), and 3(b)), which overall leads to an effective charge of

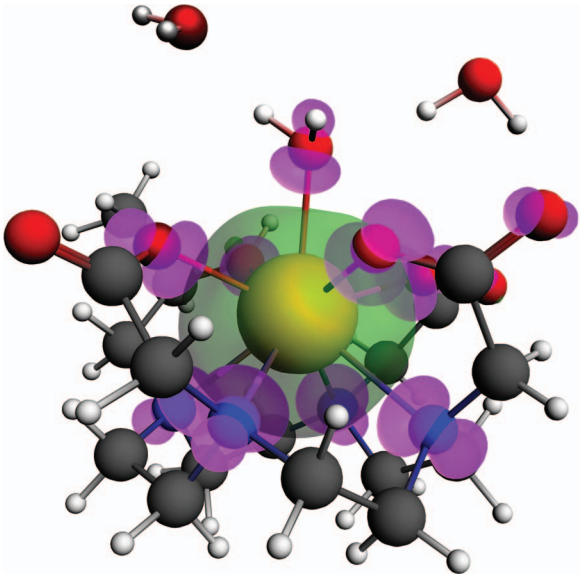

FIG. 2. Spin density isosurfaces for [Gd(HPDO3A)(H_2O)] (in green for ρ_α and pink for ρ_β contributions) and two SS water molecules revealing nearly spherical contribution on Gd together with ligands lone pairs.

+2.06 on Gd along the AIMD trajectory according to a Mulliken analysis. As already stated by Glendening *et al.*,[29] these electron transfers are favored by the stabilization of the $5d_\alpha$ spinorbitals interacting with the occupied $4f_\alpha$ spinorbitals.

As for the dipolar components, the same tendencies apply in a larger extent since nonlocal contributions are also taken into account. Table I presents the average value and fluctuations of the a_{zz} component of the dipolar tensor along its instantaneous longitudinal principal axe. Although the short-time dynamics is mainly governed by the ultrafast vibrations of the chelate (see hereafter for a detailed analysis), it is also significantly altered by the formation of hydrogen bonds between the IS and solvent molecules. Since H1 is much more frequently involved in this kind of interaction, the fluctuations of the longitudinal component of its hyperfine tensor are much more constrained (see Fig. 4). As shown hereafter, this will cause a slower loss of correlation for H1 than for H2.

Validity of the point-dipole approximation

Before we discuss magnetodynamical properties, we would like to mention a few words about the applicability of

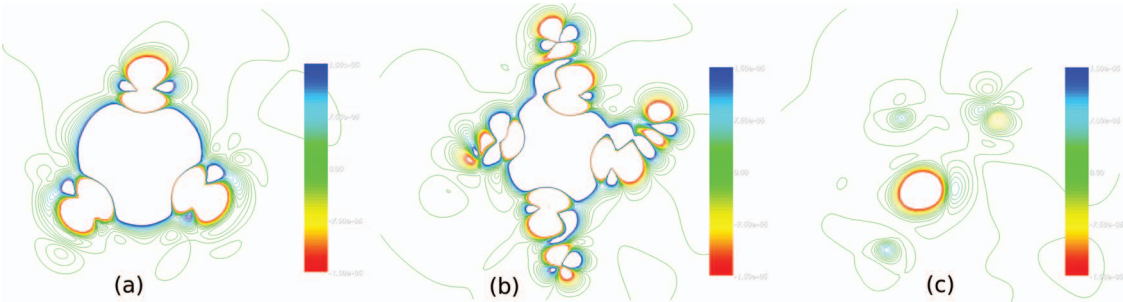

FIG. 3. Spin density contours in cutplanes for [Gd(HPDO3A)(H_2O)] showing (a) Gd (at center), IS water lone pairs (on top), and two nitrogens lone pairs (at bottom left and right); (b) Gd (at center), all carboxylate oxygens lone pairs (on top, at middle right, and bottom), and OH lone pairs at middle left; and (c) two SS water (on top left and at bottom), IS water (at center), and one carboxylate oxygen (on top right).

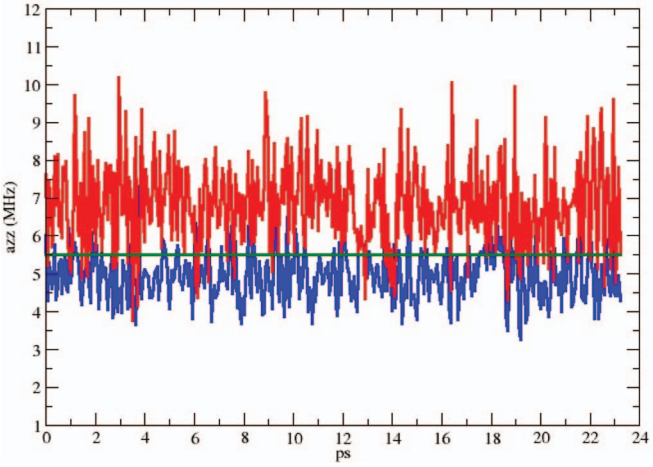

FIG. 4. Time fluctuations of the longitudinal component of the hyperfine tensor (on the instantaneous principal axes) for H1 (in blue) and H2 (in red) atoms of IS water in [Gd(HPDO3A)(H_2O)]. The experimental value[27] of 5.5 MHz is represented by the green line.

the point-dipole approximation since it could be of interest for the interpretation of experimental NMR spectra. If the electron density distribution is grossly approximated by a Dirac peak centered on Gd, the calculation of the anisotropic hyperfine tensor is straightforward (while isotropic contributions on IS water simply vanish). For example, if the coordinate system is chosen such that Gd and the atom n are both on the x-axis, Eqs. (4) and (5) simplify to

$$a^{dip}_{n,xx} = 2g\beta g_n\beta_p/r^3_{Gdn}, \tag{12}$$

$$a^{dip}_{n,xy} = -1g\beta g_n\beta_p/r^3_{Gdn}. \tag{13}$$

The averaged isotropic values reported in Table I reveal that the PD approximation will probably be much more accurate for H1 than for H2 or O_w. From their study of [Gd(DOTA)(H_2O)]$^-$ in water, Yazyev *et al.* already came to the conclusion that this approximation could only describe hyperfine interactions between Gd and a water proton.[12] For the water oxygen, they recommend a correction of the Gd-O_w distance by using a prefactor of 1.0625 in order to compensate for the overestimation of the dipolar interactions due to the absence of electron spin density delocalization. From our trajectory, we find a corresponding prefactor of 1.0612. This excellent agreement is particularly striking since both values derive from the studies of different ligands (DOTA versus HPDO3A) using distinct computational approaches (classical versus *ab initio* MDs).

Although the instantaneous hyperfine tensors may be well approximated by the point dipole approximation, non-axial fluctuations of the positions of the atoms of the IS water molecule can result in a vibrationally average hyperfine tensor that has three non-equal eigenvalues. We have thus computed the average hyperfine tensors of the three atoms of the IS molecule along the whole dynamics, in the molecular frame. The CA molecular frame was obtained by aligning the heavy atoms of Prohance, including gadolinium but excluding all water molecules even the inner shell water, onto a reference configuration. The reference configuration was taken as the Prohance configuration in the first frame; other choices (average atomic positions along the dynamics) lead to identical results. Table II shows the eigenvalues of the vibrationally averaged hyperfine tensors for atoms O, H_1, and H_2 of the IS water molecule. It can be seen that in all three cases, two eigenvalues are very close, justifying the use of the point dipole approximation for the vibrationally averaged hyperfine tensor entering expression of relaxivities.

TABLE II. Averaged eigenvalues of hyperfine tensors of oxygen and hydrogens IS water molecule.

Axis	Oxygen	Hydrogen H_1	Hydrogen H_2
XX	0.559	− 2.461	− 3.192
YY	0.530	− 2.396	− 3.294
ZZ	− 1.089	4.857	6.486

Hyperfine interaction of Gd^{3+} with OS water molecules

Fries[30] relates the relaxation rate of the OS water protons to a dipolar time correlation function, denoted $g_2^{OS}(t)$, whose initial value, $g_2^{OS}(0)$, is a structural quantity involving the radial pair distribution function of OS water protons:

$$g_2^{OS} = \int dr\, 4\pi r^2 \rho_H g(r) \times \frac{1}{r^6}, \tag{14}$$

where ρ_H is the density of protons in the solvent, and $g(r)$ is the pair distribution function of OS protons around Gd^{3+}. The relation of the OS relaxivity to such structural quantity has been used for structural determination using paramagnetic relaxation enhancement. In particular, it has been shown that if Gd^{3+} is replaced by another lanthanide with $L \neq 0$, the fast electronic spin relaxation makes g_2^{OS} directly accessible to experiment.[30] This quantity is readily accessible from the simulation and we have computed $g_2^{OS}(0)$ from our AIMD simulation with explicit water molecules and found $g_2^{OS} = 1.73 \times 10^{-3}$ Å^{-6}. It is interesting to note that this quantity, involving protons from the bulk, is of the same order of magnitude as the average $\frac{1}{r^6}$ quantity for the two IS protons (9.87×10^{-4} Å^{-6} for H_1 and 1.84×10^{-3} Å^{-6} for H_2).

Time autocorrelation functions and spectral densities

In the extreme narrowing regime that is sampled during our AIMD simulation, only short-time properties can be studied. We consider the time autocorrelation functions of the spatial part of the dipolar interactions $a^{dip}_{n,\lambda\mu}$ (which is assumed to be separated from the electron spin part according to the decomposition approximation)

$$C_{n,\lambda\mu}(t) = \frac{\left\langle a^{dip}_{n,\lambda\mu}(t) \cdot a^{dip}_{n,\lambda\mu}(0)\right\rangle}{\left\langle a^{dip}_{n,\lambda\mu}(0) \cdot a^{dip}_{n,\lambda\mu}(0)\right\rangle}. \tag{15}$$

Since only the spin relaxation of protons is relevant in MRI images, the PD approximation has been used in order to

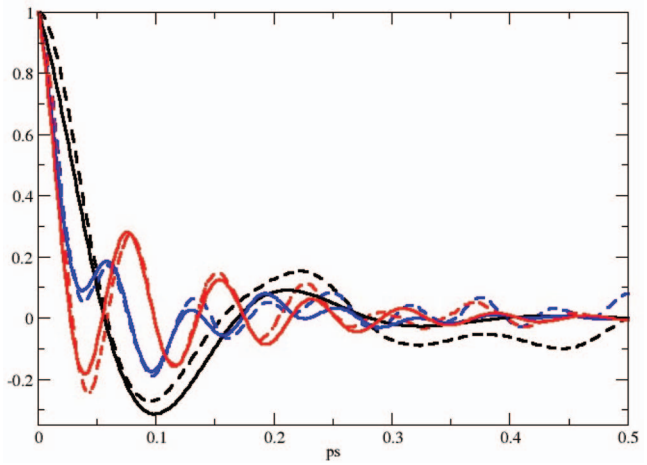

FIG. 5. Autocorrelation function of the longitudinal component of the hyperfine tensor in the PD approximation for O_w (in black), H_1 (in blue), and H_2 (in red). Dashed lines for the PD approximation curves and solid ones for the fit.

reduce the computational cost and calculate time autocorrelation functions along the whole AIMD trajectory. In spite of better statistics, these calculations, reported in Fig. 5, have hardly converged. Each data set has therefore been fitted by a linear combination of exponentially decaying cosine functions:

$$C_{O,zz}(t) = \exp(-t/a_0)\cos(2t\pi/a_1), \tag{16}$$

$$C_{H1,zz}(t) = (1-a_3)\exp(-t/a_2) + a_3\exp(-t/a_0) \times \cos(2t\pi/a_1) \times \cos(2t\pi/a_4), \tag{17}$$

$$C_{H2,zz}(t) = (1-a_3)\exp(-t/a_2) + a_3\exp(-t/a_0)\cos(2t\pi/a_1), \tag{18}$$

with $a_0 = 0.091$ and $a_1 = 0.225$ for O_w, $a_0 = 0.11$, $a_1 = 0.099$, $a_2 = 0.033$, $a_3 = 0.49$, and $a_4 = 0.18$ for H1, and $a_0 = 0.116$, $a_1 = 0.078$, $a_2 = 0.030$, and $a_3 = 0.462$ for H2.

Integrating under each of these curves leads to the following correlation times: $\tau_{O_w} = 12$ fs, $\tau_{H_1} = 19$ fs, and $\tau_{H_2} = 17$ fs. Beside the faster loss of correlation for the oxygen atom, a shorter correlation time is obtained for the "free" H_2 atom in comparison with H_1, as expected from our previous hydrogen bond analysis. This different dynamics for the two hydrogen atoms will be discussed later. In order to describe the dynamics of the "constrained" H_1 atom, and especially the minimum of $C_{H_1,zz}(t)$ located at 0.04 ps, please note that two cosine functions have been used in Eq. (17).

In a second step, so as to get a better estimation of O_w correlation time, a set of full electronic structure calculations have been performed instead of using PD approximation, and the results were fitted in the same way. Since the calculated value is identical to the PD one, the time scale of IS oxygen correlation time can be safely estimated to a dozen of fs.

Spin-lattice relaxation times T_1 are actually calculated in terms of spectral density functions, which are Fourier

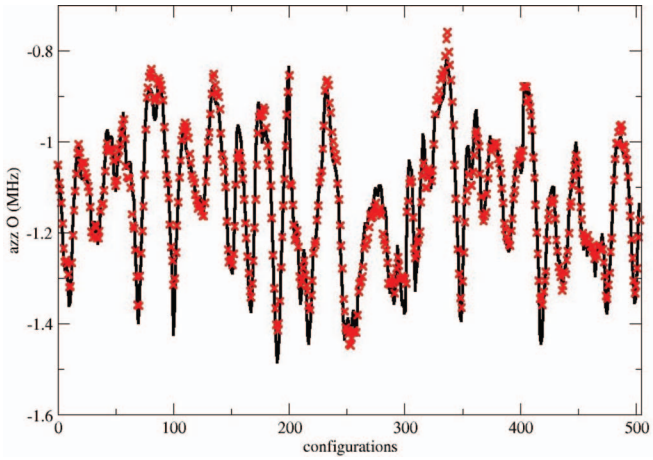

FIG. 6. Values of a_{zz} from quantum calculations (red) and decomposition method (black).

transforms of $C_{n,\lambda\mu}(t)$. Although our short CP trajectories cannot capture the molecular motions which are mainly responsible for NMR transitions (e.g., the molecular tumbling), spectral density functions can be calculated to reveal which vibrational motions govern the short-time fluctuations of hyperfine interactions. To pursue along this line and to allow for the interpretation of the spectra, we have first reconstructed the whole dynamics of the hyperfine tensor from the decomposition of the calculated values using a set of relevant CVs. The decomposition was obtained in the case of the PD approximation, and then in the full-quantum calculations case, but always using the χ^2 method presented above (see Eq. (7)).

As an illustration of the quality of the procedure, Figs. 6 and 7 present a comparison between the quantum calculations or point dipole approximation to the hyperfine tensor of the oxygen atom, respectively, and the reconstructed values from the collective variables. In Fig. 6, the configuration indexes do not correspond to time along the dynamics since the quantum calculations of the hyperfine tensors were performed only for parts of trajectory (see above). These two graphs demonstrate that the reconstruction is able to fully

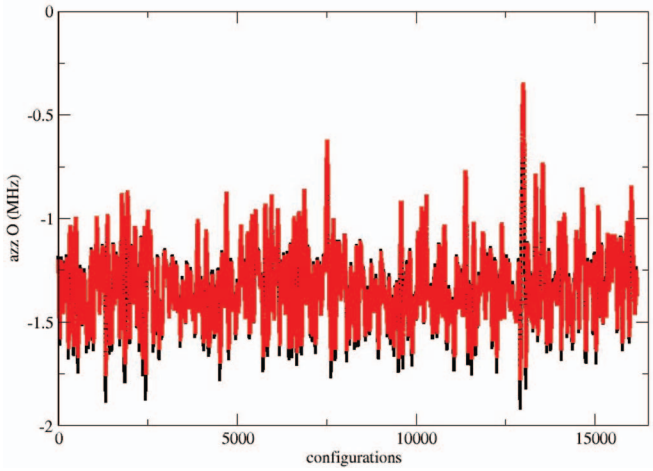

FIG. 7. Values of a_{zz} from PD approximation (red) and decomposition method (black).

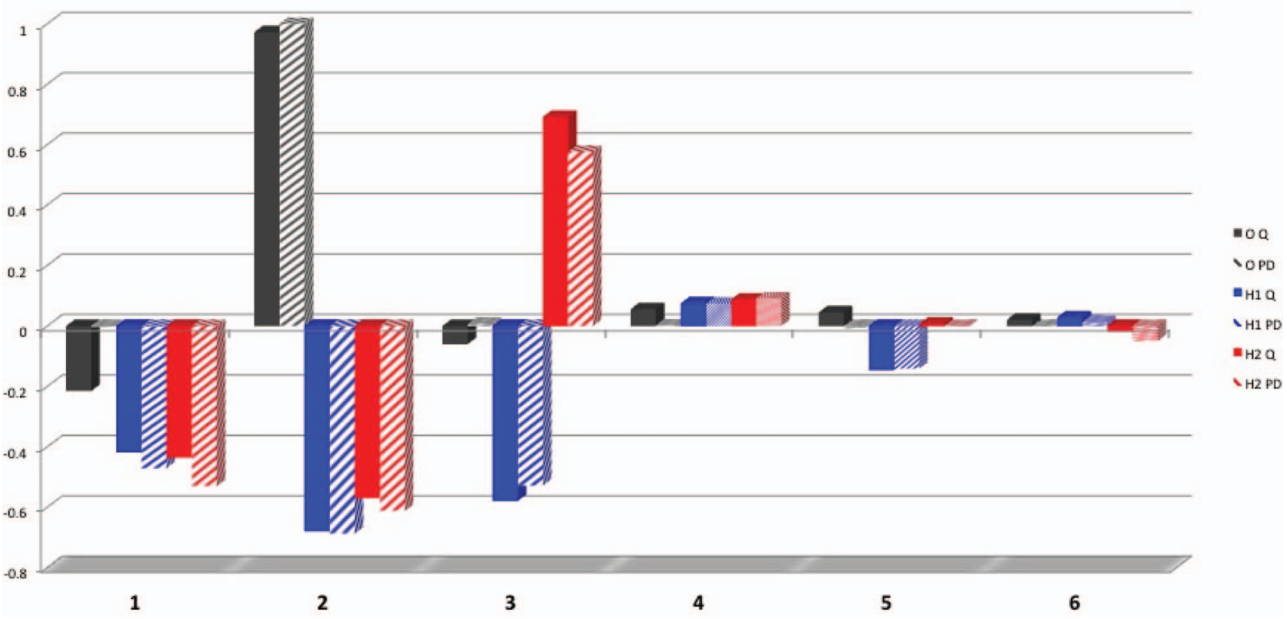

FIG. 8. Decomposition of the longitudinal spectral densities of O_w (in grey), H_1 (in blue), and H_2 (in red) in terms of normalized weights of six collective variables, namely, an out-of-plane motion, Gd–O_w, (GdO_wH$_1$)-(GdO_wH$_2$), (H$_1$O$_w$H$_2$), O_w–H_1, O_w–H_2. Plain for quantum results and dashed for PD results.

catch the fluctuations of the hyperfine tensors. Only for extreme values a deviation with the target value can be observed. This is due to the limitation of our reconstruction to linear order in the collective variables.

Fig. 8 then shows the relative weights of each CVs in the decomposition of the hyperfine tensors of O_w, H_1, and H_2 in the two cases. First, it can be observed that the decomposition of either the quantum values or point dipole approximation of the hyperfine tensors agrees qualitatively and even quantitatively up to a few percents. While fluctuations of the longitudinal component of dipolar hyperfine interactions of the oxygen atom seem to be only governed by the Gd–O_w distance (i.e., second CV), the other five CVs are required to describe precisely these fluctuations in the case of hydrogen atoms. At this level, the two hydrogen atoms appear in fact nearly equivalent with approximatively the same weights on OH distances and the three angles describing the water molecule orientation. Only the sign of the third CV is different because of its definition. As will be seen later, the main difference lies in the dynamics of the two OH stretches.

From the spectral density of each of the CVs, shown in Fig. 9, a reconstruction of the longitudinal component of the hyperfine tensor extrapolated to the whole trajectory is then made possible using the weights obtained in the quantum calculations decomposition. Such procedure will allow us to combine the accuracy of the quantum description and the statistics of the PD approximation. As a check the reconstructed longitudinal spectral densities fit for the hydrogen behaviour with the one issued from PD approximation (see Fig. 9). For each of the atoms of the IS water molecule, three well-defined peaks can be observed in the far (900–0 cm^{-1}) and mid-infrared (4000–900 cm^{-1}) regions. From comparison with IR experimental spectra,[31,32] these bands seem to correspond to librations, bending, and stretching modes of the IS water molecule, respectively. Our spectral decomposition enables us to analyse unambiguously the contribution of the different collective variables thanks to their weights $w_{n,i}$.

We thus now proceed to the assignment of the peaks in the reconstructed spectral density. The oxygen peaks could be assigned, respectively, to θ_2 (the Gd–O_w distance) and θ_4 ((H$_1$O$_w$H$_2$) angle). The inequivalence of the two hydrogens is here better observed. Concerning the hydrogen H_2, which is the one less involved in hydrogen bonds, the peaks could be assigned, respectively, to θ_2, θ_3, θ_4, and θ_6, while

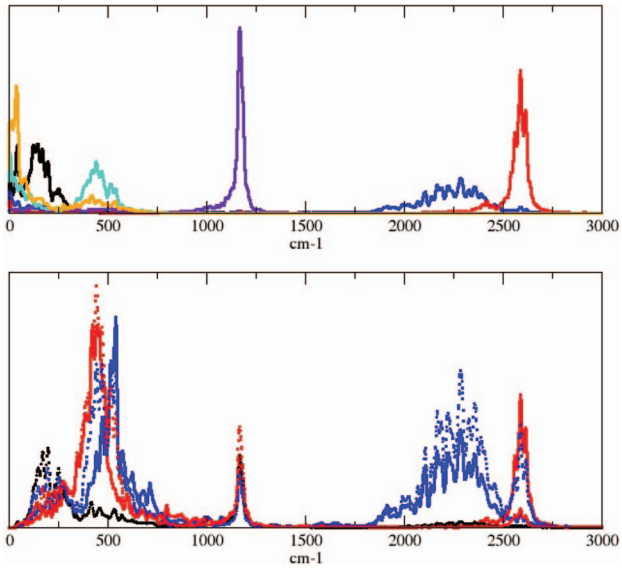

FIG. 9. Top: densities of states of the collectives variables θ_1 (in orange), θ_2 (in black), θ_3 (in turquoise), θ_4 (in violet), θ_5 (in blue), and θ_6 (in red). Bottom: reconstructed spectral densities with quantum weights of the longitudinal components of O (in black dotted), H_1 (in blue dotted), and H_2 (in red dotted), together with spectral densities in the PD case for H_1 (in blue full line) and H_2 (in red full line).

the CV's contributions to the fluctuations of H_1 would be θ_2, θ_3, θ_4, θ_5, and to a lesser extent, θ_6. CV value associated to θ_5 is redshifted with respect to θ_6 by about 300 cm^{-1} and its spectral density is characteristic of an hydrogen bonded water molecule. The approximation of the spectral density catches the difference of behaviour of the two hydrogens. It appears that the two hydrogens are quite sensitive to the internal geometry of the water molecule, and a frequency shift is observed between H_1 and H_2 due to the hydrogen bonds.

The projection of the decomposition method can help to understand the difference between PD and quantum results for oxygen. In the latter case, CV values associated to internal molecular geometry of the water molecule are in fact important in the description of the tensor, but are not included in the PD approximation. Nevertheless, the most important CV concerns the gadolinium oxygen distance with a relative intensity of the band around 55%, so it appears that this distance is not properly described. As an attempt to solve this problem, some other CV values were introduced in the decomposition model, as, for example, the presence of hydrogen bonds, but with no remarkable results. Actually, the problem of gadolinium-oxygen distance definition is not due to an electronic transfer from the environment to the water molecule, but probably an impact of gadolinium atom on the oxygen (i.e., polarization).

CONCLUSION

The high-frequency modulations of the hyperfine interactions between a Gd(III)-based MRI contrast agent and water have been modeled by a state-of-the-art AIMD simulation. The trajectory has first revealed that the two IS water protons are subjected to distinct dynamics owing to the formation of hydrogen bonds with SS solvent molecules. This behavior not only affects the internal geometry of the complex but also the high-frequency part of the spectral densities. The equivalence of the two protons in the NMR signal then stems from fast exchange, which averages the two contributions. These differences should be taken into account for a fine detailed interpretation of NMR experimental data or for theoretical predictions of magnetic properties that are only based on geometry optimizations with only a few explicit solvent molecules since both approaches used to assume essentially equivalent protons.

In addition, the decomposition method used in this work has revealed the nature of the vibrational motions which are responsible for the high-frequency part of the power spectrum. Although these motions are too fast to be probed by NMR, our analysis confirms that the collective variables involved in these ultrafast vibrations are related to librations, stretching, and bending modes of the IS water molecule. Moreover, the influence of the hydrogen bonds network on these vibrational motions has been clearly observed.

ACKNOWLEDGMENTS

This work was performed using HPC resources from GENCI-CCRT and IDRIS (Grant 2012-072195). It was supported by the EC COST Action D-38 Metal-Based Systems for Molecular Imaging Applications.

[1] J. Kowalewski and L. Mäler, *Nuclear Spin Relaxation in Liquids: Theory, Experiments, and Applications* (Taylor and Francis Group, New York, 2006).
[2] E. Tóth, L. Helm, and A. E. Merbach, Top. Curr. Chem. **221**, 61 (2002).
[3] G. Lipari and A. Szabo, J. Am. Chem. Soc. **104**, 4546 (1982).
[4] G. Lipari and A. Szabo, J. Am. Chem. Soc. **104**, 4559 (1982).
[5] S. Sýkora, J. Vogt, H. Boesiger, and P. Diehl, J. Magn. Reson. **36**, 53 (1979).
[6] E. R. Henry and A. Szabo, J. Chem. Phys. **82**, 4753 (1985).
[7] J. Kowalewski, M. Effemey, and J. Jokisaari, J. Magn. Reson. **157**, 171 (2002).
[8] D. Marx and J. Hutter, *Ab Initio Molecular Dynamics: Basic Theory and Advanced Methods* (Cambridge University Press, Cambridge, 2009).
[9] J. Hutter *et al.*, CPMD Software Package, see www.cpmd.org.
[10] B. Kirchner, P. J. di Dio, and J. Hutter, Top. Curr. Chem. **307**, 109 (2012).
[11] O. Yazyev and L. Helm, Eur. J. Inorg. Chem. **2**, 201 (2008).
[12] O. Yazyev, L. Helm, V. Malkin, and O. Malkina, J. Phys. Chem. A **109**, 10997 (2005).
[13] R. Pollet, N. Nair, and D. Marx, Inorg. Chem. **50**, 4791 (2011).
[14] R. McWeeny, *Spins in Chemistry* (Dover, New York, 2004).
[15] N. Nair, E. Schreiner, R. Pollet, V. Staemmler, and D. Marx, J. Chem. Theory Comput. **4**, 1174 (2008).
[16] M. Martinez, M.-P. Gaigeot, D. Borgis, and R. Vuilleumier, J. Chem. Phys. **125**, 144106 (2006).
[17] J. P. Perdew, K. Burke, and M. Ernzerhof, Phys. Rev. Lett. **77**, 3865 (1996); **78**, 1396 (1997) (Erratum).
[18] D. Vanderbilt, Phys. Rev. B **41**, 7892 (1990).
[19] ADF2013, SCM, Theoretical Chemistry, Vrije Universiteit, Amsterdam, The Netherlands, see http://www.scm.com.
[20] G. te Velde, F. M. Bickelhaupt, S. J. A. van Gisbergen, C. F. Guerra, E. J. Baerends, J. G. Snijders, and T. Ziegler, J. Comput. Chem. **22**, 931 (2001).
[21] C. F. Guerra, J. G. Snijders, G. te Velde, and E. J. Baerends, Theor. Chem. Acc. **99**, 391 (1998).
[22] See supplementary material at http://dx.doi.org/10.1063/1.4820791 for benchmarks related to the choice of the density functional, the relativistic treatment, and the size of the system.
[23] E. van Lenthe, A. van der Avoird, and P. E. S. Wormer, J. Chem. Phys. **108**, 4783 (1998).
[24] F. Neese, Comput. Mol. Sci. **2**, 73 (2012).
[25] K. Kumar, C. A. Chang, L. C. Francesconi, D. D. Dischino, M. F. Malley, J. Z. Gougoutas, and M. F. Tweedle, Inorg. Chem. **33**, 3567 (1994).
[26] D. Esteban-Gomez, A. de Blas, T. Rodriguez-Blas, L. Helm, and C. Platas-Iglesias, ChemPhysChem **13**, 3640 (2012).
[27] A. V. Astashkin, A. M. Raitsimring, and P. Caravan, J. Phys. Chem. A **108**, 1990 (2004).
[28] S. Laurent, L. V. Elst, and R. N. Muller, Contrast Med. Mol. Imaging **1**, 128 (2006).
[29] E. D. Glendening and P. A. Petillo, J. Phys. Chem. B **105**, 1489 (2001).
[30] P. Fries, J. Chem. Phys. **136**, 044504 (2012).
[31] J.-J. Max and C. Chapados, J. Chem. Phys. **131**, 184505 (2009).
[32] S. Y. Venyaminov and F. G. Prendergast, Anal. Biochem. **248**, 234 (1997).